

Helicity-dependent parton distribution functions at next-to-next-to-leading order accuracy from inclusive and semi-inclusive deep-inelastic scattering data

Valerio Bertone^a, Amedeo Chiefa^{b,c}, and Emanuele R. Nocera^c

(MAP Collaboration)¹

^a IRFU, CEA, Université Paris-Saclay, F-91191 Gif-sur-Yvette, France

^b The Higgs Centre for Theoretical Physics, University of Edinburgh,
JCMB, KB, Mayfield Rd, Edinburgh EH9 3JZ, Scotland

^c Università degli Studi di Torino and INFN, Torino,
Via P. Giuria 1 I-10125 Torino, Italy

Abstract

We present MAPPDFPOL1.0, a new determination of the helicity-dependent parton distribution functions (PDFs) of the proton from a set of longitudinally polarised inclusive and semi-inclusive deep-inelastic scattering data. The determination includes, for the first time, next-to-next-to-leading order QCD corrections to both processes, and is carried out in a framework that combines a neural-network parametrisation of PDFs with a Monte Carlo representation of their uncertainties. We discuss the quality of the determination, in particular its dependence on higher-order corrections, on the choice of data set, and on theoretical constraints.

1 Introduction

The accurate and precise determination of helicity-dependent (polarised, henceforth) proton parton distribution functions (PDFs) [1] is key to understand the quark and gluon spin structure of the nucleon [2]. This endeavour, which started more than thirty years ago with the first measurements of the spin-dependent structure function g_1 in polarised inclusive deep-inelastic scattering (DIS) by the European Muon Collaboration [3, 4], is the focus of the forthcoming Electron-Ion Collider (EIC) experimental program [5, 6]. The EIC, which is expected to start operating in the 2030s, will collide proton and lepton beams, with the possibility of polarising them both. Spin asymmetries for longitudinally polarised inclusive DIS and semi-inclusive DIS (SIDIS) will be measured for a range of proton momentum fractions x and electroweak boson virtualities Q^2 that will significantly extend those accessed by current measurements (see *e.g.* Fig. (1) in Ref. [1]). The precision of these measurements will be unprecedented and is forecast to attain the percent level (see *e.g.* Sect. II in Ref. [7]).

The precision of future EIC measurements calls for a matching accuracy of the corresponding theoretical predictions. Perturbative corrections to the massless polarised inclusive DIS structure function g_1 have been known at next-to-next-to-leading order (NNLO) in the strong-coupling expansion, *i.e.* $\mathcal{O}(\alpha_s^2)$, for a long time [8]², and up to N³LO, *i.e.* $\mathcal{O}(\alpha_s^3)$, since very recently [10]. Massive contributions are known up to $\mathcal{O}(\alpha_s^2)$ [11], together with their asymptotic limit [12–17]. In the last

¹The MAP acronym stands for “Multi-dimensional Analyses of Partonic distributions”. It refers to a collaboration aimed at studying the three-dimensional structure of hadrons.

²Other massless polarised DIS structure functions have been recently computed up to NNLO accuracy as well [9].

two years, NNLO corrections have also been computed for the massless polarised SIDIS structure function g_1^h , albeit using an approximation based on the threshold resummation formalism [18], and for W -boson production in polarised proton–proton collisions [19].

The accuracy of theoretical predictions for spin-dependent observables, however, depends not only on the accuracy of the perturbative computations, but also on the accuracy of the PDFs that must be convolved with them. The latter are determined by comparing theoretical predictions computed with the same accuracy to the experimental data. To date, the only available polarised PDF set accurate to NNLO was determined by analysing polarised DIS data only [20]. This data is not sensitive to the decomposition of the proton spin into the separate contributions carried by quarks and antiquarks of different flavours. Hence, other polarised PDF sets [21, 22] based on more global data sets, despite being accurate only to next-to-leading order (NLO), have been more widely used so far.

In this paper we present MAPPDFPOL1.0, a global analysis of polarised PDFs accurate to NNLO based on DIS and SIDIS data. We utilise a fitting framework similar to that developed in two previous works in which we determined the pion and kaon Fragmentation Functions (FFs) [23, 24]. This framework combines a neural-network parametrisation of polarised PDFs (optimised through knowledge of the analytical derivative of neural networks with respect to their parameters) with a Monte Carlo representation of PDF uncertainties. This approach — which has been extensively used by the NNPDF Collaboration to determine the unpolarised/polarised proton and nuclear PDFs and the FFs (see *e.g.* Refs. [22, 25–27] and references therein) — allows one to reduce the parametrisation bias as much as possible and to faithfully propagate experimental uncertainties into PDFs. We carefully assess the impact of NNLO corrections, data sets, and theoretical constraints on the polarised PDFs and their uncertainties. In particular, we test possible violations of the SU(2) and SU(3) flavour symmetries, the effect of positivity constraints, and, for the first time, whether SIDIS data combined with NNLO corrections allow one to determine an asymmetry between polarised strange and antistrange PDFs.

The structure of the paper is as follows. In Sect. 2 we present the experimental data analysed in this work. In Sect. 3 we discuss the details of the corresponding theoretical computations. In Sect. 4 we review the methodological aspects of the analysis, focusing on those that are peculiar to the determination of polarised PDFs. The results of our determination are presented in Sect. 5, in which we discuss in turn the impact of NNLO corrections, of data sets, and of theoretical constraints. Summary and outlook are finally given in Sect. 6. The MAPPDFPOL1.0 sets are released in the LHAPDF format [28], and the software developed to produce them is made open source [29].

2 Experimental data

This analysis is based on a comprehensive set of measurements of polarised structure functions in lepton-nucleon DIS and SIDIS. Concerning DIS, we consider data coming from the EMC [4], SMC [30], and COMPASS [31, 32] experiments at CERN, from the E142 [33], E143 [34], E154 [35], and E155 [36] experiments at SLAC, from the HERMES [37, 38] experiment at DESY, and from the Hall A [39] and CLAS [40] experiments at JLab. All of these experiments deliver data for the polarised inclusive structure function g_1 , reconstructed from the longitudinal double spin asymmetry (see Sect. 2.1 in Ref. [41] for details), except E155, Hall A, and CLAS, which instead deliver data for g_1 normalised to the unpolarised inclusive structure function F_1 . Concerning SIDIS, we consider data from COMPASS [42] and HERMES [43]. Both of these experiments deliver data for the polarised semi-inclusive structure function g_1^h , with $h = \pi^+, \pi^-, K^+, K^-$, normalised to its unpolarised counterpart F_1^h . The target in the aforementioned DIS and SIDIS data sets is a proton, or a neutron, or a deuteron.

The data set is summarised in Table 1 and its kinematic coverage in the (x, Q^2) plane is displayed in Fig. 1. The data points cover a rather limited region, roughly $0.005 \lesssim x \lesssim 0.5$ and $1 \lesssim Q^2 \lesssim 100 \text{ GeV}^2$. We apply kinematic cuts on the virtuality $Q^2 \leq Q_{\text{cut}}^2$ and on the invariant mass of the final state $W^2 = Q^2(1-x)/x \leq W_{\text{cut}}^2$. The cut on Q^2 removes a region where perturbative computations become unreliable because of the rise of the strong coupling. The cut on W^2 removes a region where leading-twist factorisation, on which we base our theoretical framework, becomes likewise insufficient. We choose $Q_{\text{cut}}^2 = 1 \text{ GeV}^2$ and $W^2 = 6.25 \text{ GeV}^2$. The first value is a common choice in

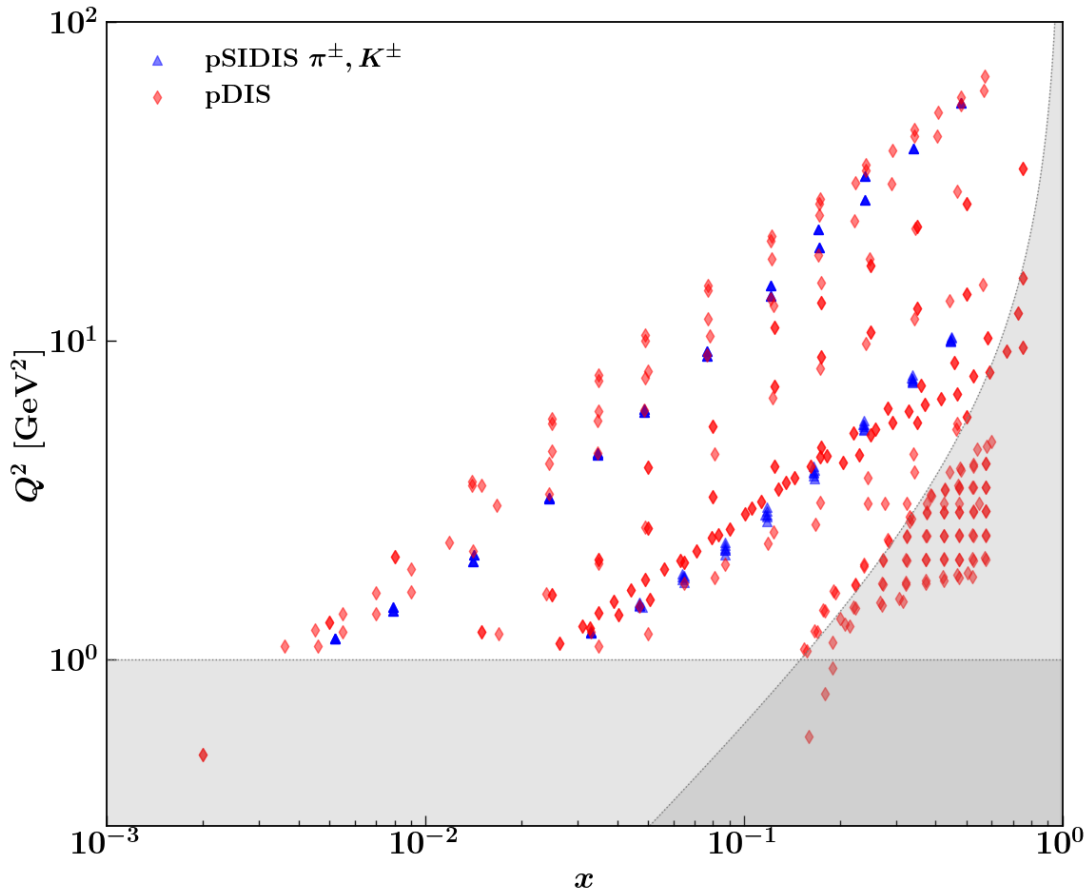


Figure 1. Kinematic coverage in the (x, Q^2) plane of the polarised DIS and SIDIS data included in this analysis. The shaded areas correspond to regions excluded by the cuts in Q^2 and W^2 , see text for more details.

several determinations of unpolarised and polarised PDFs, and results from a tradeoff between incorporating as much experimental information as possible and preserving the reliability of perturbative computations. The second value is selected among the set of values $W_{\text{cut}}^2 = 1.0, 4.0, 6.25, 9.0 \text{ GeV}^2$ after performing a fit with each of them and verifying that it maximises the fit quality and preserves the stability of PDFs in comparison to those obtained with other choices. The regions excluded by the kinematic cuts correspond to the shaded areas in Fig. 1. Note that some JLab measurements, namely those from Hall-A [44] and CLAS [45], are completely excluded by our kinematic cuts. They will therefore not be considered in the rest of this paper.

Statistical and systematic uncertainties are separately provided for each of the measurements listed in Table 1, however detailed information on correlations is missing in most cases. Specifically, for the EMC, E143, and E155 experiments a correlated multiplicative uncertainty is specified, whereas for the HERMES DIS and SIDIS experiments of Refs. [38, 43] the bin-by-bin covariance matrix is given. In all of these cases we take into account the available piece of information on experimental correlations. In the other cases, we assume the systematic uncertainties to be uncorrelated and we add them in quadrature with the statistical ones.

In addition to the aforementioned DIS and SIDIS measurements, we also optionally consider data corresponding to semi-leptonic β -decays of the baryonic octet. Assuming SU(2) and SU(3) flavour symmetries, these can be related (see *e.g.* Ref. [46]) to the lowest moments of the triplet and octet polarised PDF combinations defined as

$$a_3 = \int_0^1 dx [\Delta f_u^+(x, Q^2) - \Delta f_d^+(x, Q^2)] , \quad (1)$$

$$a_8 = \int_0^1 dx [\Delta f_u^+(x, Q^2) + \Delta f_d^+(x, Q^2) - 2\Delta f_s^+(x, Q^2)] , \quad (2)$$

where $\Delta f_q^+ = \Delta f_q + \Delta f_{\bar{q}}$. Both a_3 and a_8 are scale independent, however, for the practical purpose of computing Eqs. (1)-(2), we set $Q^2 = 1 \text{ GeV}^2$. The values that we use are $a_3 = 1.2756 \pm 0.0013$ and $a_8 = 0.585 \pm 0.025$ [47]. The impact of these data points will be discussed in Sect. 5.3.

3 Theoretical predictions

The experimental data described in Sect. 2 are measured in DIS and SIDIS processes where a polarised lepton beam scatters off a polarised nucleon target

$$\ell(k, s) + N(P, S) \longrightarrow \ell'(k') + (h^\pm(p_h)) + X. \quad (3)$$

Here P is the four-momentum of the nucleon N , k (k') is the four-momentum of the incoming (outgoing) lepton ℓ (ℓ'), and p_h is the four-momentum of the outgoing hadron h^\pm (in SIDIS); S and s are the spin four-vectors of the nucleon and incoming lepton, respectively. Because of the very moderate values of the virtuality Q^2 (see Fig. 1), the scattering involves only the exchange of a virtual photon.

The measured observables are related to the difference between cross sections with opposite target spins, which, neglecting terms suppressed by powers of M^2/Q^2 with M the nucleon mass, read

$$\begin{aligned} \text{DIS} & : \quad \frac{d\Delta\sigma}{dxdy} = \frac{1}{2} \left(\frac{d\sigma^{\rightarrow, \Rightarrow}}{dxdy} - \frac{d\sigma^{\rightarrow, \Leftarrow}}{dxdy} \right) = \frac{4\pi\alpha^2}{xQ^2} (2-y) g_1(x, Q^2), \\ \text{SIDIS} & : \quad \frac{d\Delta\sigma_h}{dxdy} = \frac{1}{2} \left(\frac{d\sigma_h^{\rightarrow, \Rightarrow}}{dxdy} - \frac{d\sigma_h^{\rightarrow, \Leftarrow}}{dxdy} \right) = \frac{4\pi\alpha^2}{xQ^2} (2-y) g_1^h(x, z, Q^2). \end{aligned} \quad (4)$$

Here \rightarrow denotes the longitudinal polarisation of the incoming lepton, parallel to its four-momentum, while \Rightarrow (\Leftarrow) denotes the longitudinal polarisations of the nucleon parallel (antiparallel) to the lepton four-momentum. The variables appearing in Eq. (4) are Lorentz invariant and are defined as follows: $Q^2 = -q^2$ is the (negative) virtuality of the photon; $x = Q^2/(2P \cdot q)$ is the (lowest) momentum fraction of the initial-state nucleon carried by the scattering parton; $z = P \cdot p_h/(P \cdot q)$ is the (lowest) momentum fraction of the fragmenting parton carried by the identified final-state hadron; and $y = P \cdot q/(P \cdot k)$ is the inelasticity, that is the energy fraction transferred by the incoming lepton.

The rightmost equalities in Eq. (4), where α is the fine-structure constant, define the polarised structure functions g_1 and g_1^h , which are reconstructed from the cross section differences measured by the experimental collaborations. Using the leading-twist collinear factorisation theorem valid for $Q^2 \gg \Lambda_{\text{QCD}}$, these structure functions factorise as³

$$g_1(x, Q^2) = \frac{1}{2} x \sum_q e_q^2 \left\{ \Delta f_q(x, Q^2) \otimes_x \Delta C_q(x, Q^2) + \Delta f_g(x, Q^2) \otimes_x \Delta C_g(x, Q^2) \right\}, \quad (5)$$

$$\begin{aligned} g_1^h(x, z, Q^2) = \frac{1}{2} x \sum_q e_q^2 \left\{ \left[\Delta f_q(x, Q^2) \otimes_x \Delta C_{qq}(x, z, Q^2) + \Delta f_g(x, Q^2) \otimes_x \Delta C_{gg}(x, z, Q^2) \right] \otimes_z D_q^h(z, Q^2) \right. \\ \left. + \Delta f_q(x, Q^2) \otimes_x \Delta C_{gq} \otimes_z D_g^h(z, Q^2) \right\}, \end{aligned} \quad (6)$$

where \otimes_w denotes the usual Mellin convolution acting on the variable w as follows:

$$C(w) \otimes_w h(w) = \int_w^1 \frac{dw'}{w'} C(w') h\left(\frac{w'}{w}\right). \quad (7)$$

In Eqs. (5) and (6) the sum runs over the quark and antiquark flavours active at scale Q^2 , e_q is the electric charge of the flavour q , ΔC are the appropriate coefficient functions, and $\Delta f_{q(g)}$ and $D_{q(g)}^h$ are

³Note that the factorised expression for the SIDIS structure function g_1^h does not include a ΔC_{gg} term proportional to both the gluon PDF Δf_g and the gluon fragmentation function D_g^h that is in principle present starting from NNLO. However, as discussed below, in our analysis we use an approximation for the NNLO corrections to SIDIS that does not include this term.

the longitudinally polarised quark (gluon) PDF of the proton and the unpolarised quark (gluon) FF of the hadron h , respectively. Since some experiments deliver data for the ratios g_1/F_1 and g_1^h/F_1^h (see Table 1), the unpolarised DIS and SIDIS structure functions F_1 and F_1^h have to be computed as well. This is done by replacing the polarised PDFs and coefficient functions Δf_i and $\Delta\mathcal{C}$ in Eqs. (5) and (6) with their unpolarised counterparts f_i and \mathcal{C} . We finally assume exact isospin symmetry to relate neutron and proton structure functions, which in turn also allows us to reconstruct the structure functions of the deuteron. No nuclear corrections are taken into account in the case of a deuterium target. Likewise, we do not consider target mass corrections.

In Eqs. (5) and (6) the coefficient functions $\Delta\mathcal{C}$ are computed as a perturbative series in the strong coupling α_s

$$\Delta\mathcal{C}(k, Q) = \sum_{n=0} \left(\frac{\alpha_s(Q^2)}{4\pi} \right)^n \Delta\mathcal{C}^{(n)}(k), \quad (8)$$

where the kinematic variable k corresponds to the initial-state momentum fraction x for DIS and to the pair of initial- and final-state momentum fractions (x, z) for SIDIS. We consider massless-quark coefficient functions up to NNLO. These were computed up to NNLO in Ref. [8] for DIS and up to NLO in Refs. [48, 49] for SIDIS. Approximate NNLO coefficient functions for SIDIS were derived in Ref. [18] by extracting the fixed-order dominant contributions associated to the emission of soft gluons close to production threshold. This approximation produces corrections only to the $\Delta\mathcal{C}_{qq}$ coefficient function. The reliability of this approximation was recently checked against the exact computation in the unpolarised case [50], finding excellent agreement.

We do not consider massive-quark corrections, which, albeit being known for g_1 up to $\mathcal{O}(\alpha_s^2)$ [11–17], are likely to be small in comparison to the size of the experimental uncertainties of the data included in the fit [51]. Intrinsic heavy-quark distributions are assumed to be identically zero below the corresponding thresholds. At higher scales, heavy-quark distributions are perturbatively generated by means of DGLAP evolution in the zero-mass variable-flavour-number scheme (ZM-VFNS).⁴ Perturbative corrections to the splitting functions entering the DGLAP equations are taken into account consistently up to NNLO accuracy [52–54].

All the expressions for the aforementioned unpolarised and polarised coefficient and splitting functions are implemented in the public code APFEL++ [55, 56], which we use to compute the theoretical predictions that enter the fit. The values of the relevant physical parameters are as follows: $\alpha_s(M_Z) = 0.118$, $m_c = 1.51$ GeV, and $m_b = 4.92$ GeV.

4 Fitting methodology

The methodological framework used to infer polarised PDFs from data is the same used to determine FFs in Refs. [23, 24]. Its main ingredients are the propagation of experimental uncertainties into polarised PDFs by means of Monte Carlo sampling, the parametrisation of PDFs by means of neural networks, and the optimisation of the parameters by means of analytic gradient descent minimisation.

Concerning the Monte Carlo sampling, all of our polarised PDF sets are made of $N_{\text{rep}} = 150$ Monte Carlo replicas. This number was chosen by requiring that the statistical features of the experimental data, namely central values, uncertainties, and correlations, be reproduced by averages, standard deviations, and covariances computed over the Monte Carlo ensemble with an accuracy below 1%.

Concerning the parametrisation, we utilise a single one-layered feed-forward neural network with one input node corresponding to the momentum fraction x , 10 intermediate nodes, and 7 output nodes, all with a sigmoid activation function. This architecture amounts to a total of 97 free parameters and

⁴We note that evolution in the VFNS requires matching conditions that encode the perturbative transition between adjacent schemes differing by one unit in the number of active quark flavours. NNLO evolution would imply the use of matching conditions accurate to $\mathcal{O}(\alpha_s^2)$. Despite the full set of $\mathcal{O}(\alpha_s^2)$ corrections to the polarised matching conditions has been recently computed in Ref. [16], they are not presented in a format readily implementable in our framework. Specifically, the expressions are presented in Mellin space, rather than in momentum space, and for heavy-quark masses renormalised in the $\overline{\text{MS}}$ scheme, rather than in the pole-mass scheme. Therefore, we use $\mathcal{O}(\alpha_s)$ matching conditions also when evolving polarised PDFs at NNLO, leaving the implementation of the $\mathcal{O}(\alpha_s^2)$ corrections for a future work.

was selected (among several with as few as 5 nodes and as many as 20 nodes in the hidden layer) as the one corresponding to a sufficiently flexible parametrisation to accommodate all data points without increasing its complexity (and thus the computational burden to train it) too much. We note that this architecture is simpler than the one used in our earlier works on FFs [23, 24] because of the comparatively scarcer and less precise measurements included in the fit.

The output nodes correspond to the independent polarised PDFs that we fit, namely

$$\{\Delta f_u, \Delta f_{\bar{u}}, \Delta f_d, \Delta f_{\bar{d}}, \Delta f_s, \Delta f_{\bar{s}}, \Delta f_g\}. \quad (9)$$

Note that, for the first time, we allow Δf_s to be different from $\Delta f_{\bar{s}}$. The availability of SIDIS data for production of positively and negatively charged kaons and of NNLO corrections, which make polarised strange quarks and antiquarks evolve differently, can in principle distinguish between the two distributions. The parametrisation scale is set to $Q_0^2 = 1 \text{ GeV}^2$.

The output layers, for each Monte Carlo replica k , are shifted and rescaled as

$$\Delta f_i^{(k)}(x, Q_0^2) = [2 \text{NN}_i(x) - 1] f_i^{(U(1,100))}(x, Q_0^2), \quad i = g, u, \bar{u}, d, \bar{d}, s, \bar{s}, \quad (10)$$

where $U(1, 100)$ is a random integer number uniformly sampled in the interval $[1, 100]$, which denotes a replica in a given unpolarised PDF set. In this way, each output node, corresponding to a replica k of each polarised PDF in the basis of Eq. (9), is bound by an unpolarised PDF replica

$$|\Delta f_i^{(k)}(x, Q_0^2)| \leq f_i^{(U(1,100))}(x, Q_0^2), \quad \forall x. \quad (11)$$

The parametrisation in Eq. (10) enforces by construction the constraint

$$|\Delta f_i(x, Q^2)| \leq f_i(x, Q^2), \quad \forall x, \forall Q^2, \quad (12)$$

which follows, at leading order (LO), from requiring positivity of cross sections

$$\begin{aligned} |g_1(x, Q^2)| &\leq F_1(x, Q^2), \\ |g_1^h(x, z, Q^2)| &\leq F_1^h(x, z, Q^2). \end{aligned} \quad (13)$$

Beyond LO, more complicated conditions hold [57, 58], however they differ only mildly from Eq. (12) at large x where they are relevant to constrain PDFs (see *e.g.* Fig. 3 in [57]). The uncertainty on the bound in Eq. (12) due to the uncertainty of the unpolarised PDF is incorporated into the polarised PDF thanks to the fact that an unpolarised PDF replica is chosen at random for each polarised PDF replica in Eq. (11). The parametrisation in Eq. (10) has two additional advantages: first, it guarantees that polarised PDFs vanish at $x = 1$ as a consequence of the fact that unpolarised PDFs also do so; second, it guarantees that polarised PDFs are integrable over x , as required to ensure the finiteness of their moments.

Whereas Eq. (10) is our default parametrisation, we have also tried the alternative implementation

$$\Delta f_i^{(k)}(x, Q_0^2) = [2 \text{NN}_i(x) - 1] \left[f_i^{(0)}(x, Q_0^2) + K \sigma_i(x, Q_0^2) \right], \quad i = g, u, \bar{u}, d, \bar{d}, s, \bar{s}, \quad (14)$$

where $f_i^{(0)}$ is the unpolarised PDF central replica, σ_i is the one-sigma unpolarised PDF uncertainty, and K is a positive integer. The larger the value of K , the looser the positivity constraint. The implementation of Eq. (14) allowed us to study how polarised PDFs depend on the positivity constraint, see Sect. 5.3.

The unpolarised PDFs entering Eqs. (10) and (14) are taken from the NNPDF3.1 [59] parton set with perturbative charm. This parton set is also used to compute the unpolarised structure functions F_1 (F_1^h) when the DIS (SIDIS) data is presented as g_1/F_1 (g_1^h/F_1^h). In the SIDIS case, a set of FFs is also needed, which we take from the MAPFF1.0 [23, 24] set.⁵ The NNPDF3.1 and MAPFF1.0 sets

⁵We use the NNPDF3.1 PDF set, despite the availability of the more recent NNPDF4.0 PDF set [25], to maximise consistency with MAPFF1.0, which used the NNPDF3.1 PDF set as input.

are respectively obtained from a global analysis of measurements in DIS and a variety of processes in proton–proton collisions, and from a global analysis of single-inclusive hadron production in electron–positron annihilation and SIDIS. Both these sets are based on a similar methodology and are accurate up to NNLO. The perturbative accuracy of the PDF and FF sets is chosen consistently with the accuracy of the analysis of polarised PDFs presented here (NLO or NNLO). In all cases, PDF and FF replicas are chosen randomly from the corresponding sets for each fitted polarised PDF replica.

Concerning the parameter optimisation, we use the exact same strategy as in Refs. [23, 24]. Specifically, for each replica: we minimise the χ^2 (see *e.g.* Eq. (21) in Ref. [23] for its definition); we adopt cross-validation with a training fraction of 80% for data sets with more than 10 points and 100% otherwise; we determine the optimal parameters with the Levenberg-Marquardt algorithm as implemented in CERES-SOLVER [60], computing the gradient of the neural network with respect to the free parameters analytically using the NNAD library [61]; and we discard replicas which, at the end of the training, result in a value of the χ^2 per data point larger than three.⁶

5 Results and discussion

We now present MAPPDFPOL1.0, the polarised PDF determination obtained from the experimental data, the theoretical predictions, and the fitting methodology described in Sects. 2–4. We discuss in turn the impact of NNLO corrections, data, and theoretical constraints by comparing fits obtained upon variations of each of these aspects to the same baseline fit. This baseline fit is obtained using NNLO theoretical predictions, the positivity constraint as in Eq. (10), and the global data set, including the measurements for a_3 and a_8 .

5.1 Impact of NNLO corrections

Table 1 reports the value of the χ^2 per data point of the NLO and NNLO MAPPDFPOL1.0 parton sets. Fit quality is generally good for both the individual and the global data sets and for both the NLO and NNLO fits. However, it worsens when including higher-order QCD corrections: the value of the global χ^2 per data point increases from 0.64 to 0.78 when moving from NLO to NNLO. This difference corresponds to about two sigma in units of the uncertainty of the expected distribution of the χ^2 . This increase is common to DIS and SIDIS data, although it is more pronounced for the latter. A similar behaviour was observed also in the case of FFs when fitting single-inclusive annihilation and SIDIS data [24, 62]. We will further investigate the interplay between higher-order corrections and the SIDIS data sets in Sect. 5.2. On the other hand, we remark that the global χ^2 per data point at both NLO and NNLO remains significantly smaller than the expectation, *i.e.* one. This fact, which was already observed in previous NLO analyses [22, 41, 63, 64] is ascribed to a very limited knowledge of experimental correlations, which may result in an effective uncertainty overestimate and lead to an anomalously small value of the χ^2 . However, it is interesting to observe that this value remains small even for the HERMES DIS data [38] for which the complete experimental covariance matrix is available and used in our fits.

In Fig. 2, we display the Δf_u , $\Delta f_{\bar{u}}$, Δf_d , $\Delta f_{\bar{d}}$, Δf_s , $\Delta f_{\bar{s}}$, Δf_c , and Δf_g PDFs from the MAPPDFPOL1.0 NNLO and NLO PDF sets as functions of x at $Q^2 = 10 \text{ GeV}^2$. Error bands correspond to one-sigma uncertainties. The impact of NNLO corrections on PDF central values is generally small in comparison to their uncertainties: Δf_u is enhanced by about half a sigma around $x \sim 0.3$; $\Delta f_{\bar{u}}$ is also enhanced by about half a sigma around $x \sim 0.1$; Δf_s and $\Delta f_{\bar{s}}$ are suppressed by slightly less than one sigma for $x \gtrsim 0.01$; and Δf_c and Δf_g are also suppressed by half a sigma around $x \sim 0.1$. Uncertainties remain almost unaffected by the inclusion of NNLO corrections, except in the case of Δf_g (and similarly of Δf_c), for which they reduce slightly.

In general, the fitted data set is not able to constrain all the parametrised PDFs to the same level of precision. While DIS data constrains Δf_u and Δf_d rather well, SIDIS data provides limited input on quark flavour separation: $\Delta f_{\bar{u}}$ and $\Delta f_{\bar{d}}$ remain compatible with zero within uncertainties at both NLO

⁶These outliers typically occur once or twice every hundred replicas.

Experiment	Ref.	Observable	N_{dat}	baseline χ^2/N_{dat}		no a_3, a_8 χ^2/N_{dat}		no pos. χ^2/N_{dat}	
				NLO	NNLO	NLO	NNLO	NNLO	
EMC	[4]	g_1^p	10	0.57	0.49	0.59	0.55	0.53	
SMC	[30]	g_1^p	12	0.29	0.32	0.31	0.29	0.29	
	[30]	g_1^d	12	1.34	1.20	1.35	1.19	1.27	
E142	[33]	g_1^n	7	0.58	0.85	0.58	0.77	0.62	
E143	[34]	g_1^p	25	0.74	0.69	0.74	0.68	0.54	
	[34]	g_1^d	25	1.30	1.23	1.28	1.25	1.32	
E154	[35]	g_1^n	11	0.22	0.20	0.23	0.22	0.31	
E155	[36]	g_1^p/F_1^p	22	0.66	0.85	0.66	0.79	0.93	
	[36]	g_1^d/F_1^d	22	0.71	0.81	0.71	0.82	0.90	
COMPASS	[32]	g_1^p	17	0.58	0.95	0.52	0.73	0.61	
	[31]	g_1^d	15	0.36	1.02	0.31	0.84	0.62	
HERMES	[37]	g_1^n	8	0.22	0.27	0.22	0.25	0.20	
	[38]	g_1^p	14	0.46	0.53	0.49	0.52	0.50	
	[38]	g_1^d	14	0.63	0.74	0.68	0.71	0.77	
JLAB-E06	[39]	g_1^n/F_1^n	1	0.72	0.86	0.69	0.82	0.51	
JLAB-EG1	[40]	g_1^p/F_1^p	2	0.01	0.01	0.01	0.01	0.01	
	[40]	g_1^d/F_1^d	1	0.01	0.01	0.01	0.01	0.01	
Total DIS			218	0.48	0.55	0.48	0.53	0.52	
COMPASS	[42]	$g_1^{p,\pi^+}/F_1^{p,\pi^+}$	12	2.32	2.01	2.33	1.94	1.38	
	[42]	$g_1^{p,\pi^-}/F_1^{p,\pi^-}$	12	1.34	1.13	1.29	1.09	0.91	
	[42]	$g_1^{p,K^+}/F_1^{p,K^+}$	12	0.69	0.94	0.77	0.97	0.82	
	[42]	$g_1^{p,K^-}/F_1^{p,K^-}$	12	0.73	0.98	0.65	0.88	0.92	
	[42]	$g_1^{d,\pi^+}/F_1^{d,\pi^+}$	10	0.31	1.23	0.31	1.38	0.50	
	[42]	$g_1^{d,\pi^-}/F_1^{d,\pi^-}$	10	0.47	1.51	0.49	1.50	0.63	
	[42]	$g_1^{d,K^+}/F_1^{d,K^+}$	10	0.40	0.40	0.28	0.24	0.34	
	[42]	$g_1^{d,K^-}/F_1^{d,K^-}$	10	0.92	0.82	0.88	0.70	0.79	
	HERMES	[43]	$g_1^{p,\pi^+}/F_1^{p,\pi^+}$	9	1.90	2.05	1.87	1.79	1.88
		[43]	$g_1^{p,\pi^-}/F_1^{p,\pi^-}$	9	1.03	0.68	1.00	0.65	0.72
[43]		$g_1^{d,\pi^+}/F_1^{d,\pi^+}$	9	0.35	1.53	0.34	1.41	0.82	
[43]		$g_1^{d,\pi^-}/F_1^{d,\pi^-}$	9	1.30	2.41	1.37	2.16	1.71	
[43]		$g_1^{d,K^+}/F_1^{d,K^+}$	9	1.48	1.72	1.46	1.65	1.89	
[43]		$g_1^{d,K^-}/F_1^{d,K^-}$	9	0.63	1.04	0.64	1.06	0.65	
Total SIDIS			142	1.00	1.31	0.99	1.23	0.99	
Total			362	0.64	0.78	0.63	0.74	0.66	

Table 1. The data sets, number of data points, and χ^2 per data point for the MAPPDFPOL1.0 PDF sets. We display the values obtained from the baseline NLO and NNLO fits, from the NLO and NNLO fit variants without data for a_3 and a_8 , and from the NNLO fit variant with a very loose positivity constraint, see Sect. 5.3. The χ^2 values are displayed for the individual and global data sets.

and NNLO; Δf_s and $\Delta f_{\bar{s}}$ are also compatible with zero within uncertainties and very similar to each other at both NLO and NNLO. In this last respect, we conclude that the currently available SIDIS

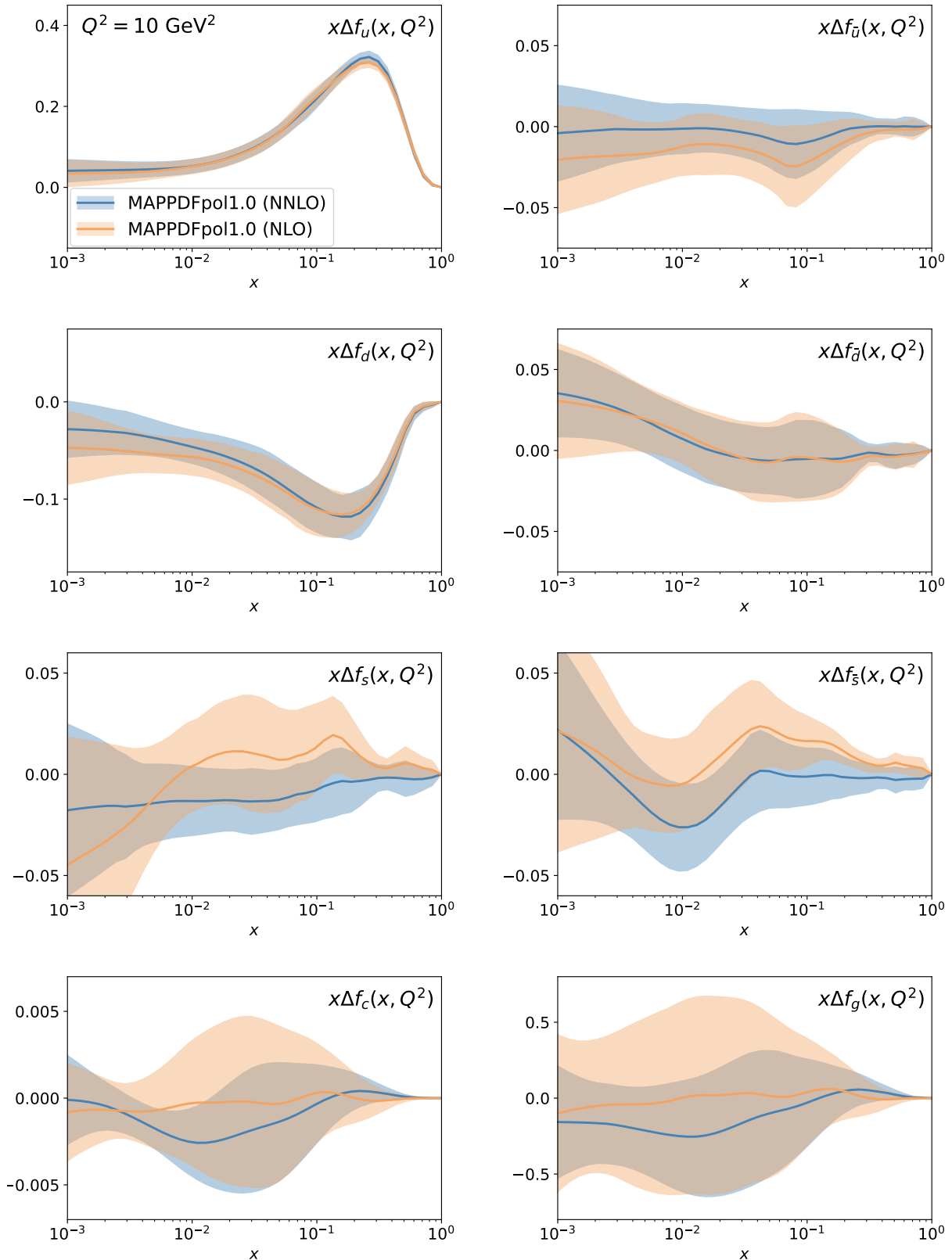


Figure 2. The Δf_u , $\Delta f_{\bar{u}}$, Δf_d , $\Delta f_{\bar{d}}$, Δf_s , $\Delta f_{\bar{s}}$, Δf_c , and Δf_g PDFs as functions of x at $Q^2 = 10 \text{ GeV}^2$ from the MAPPDFPOL1.0 NLO and NNLO PDF sets. Error bands correspond to one-sigma uncertainties.

data, even when analysed including NNLO corrections, is unable to pin down a possible polarised strange asymmetry. Finally, DIS and SIDIS data leave Δf_g and Δf_c , the latter generated by gluon

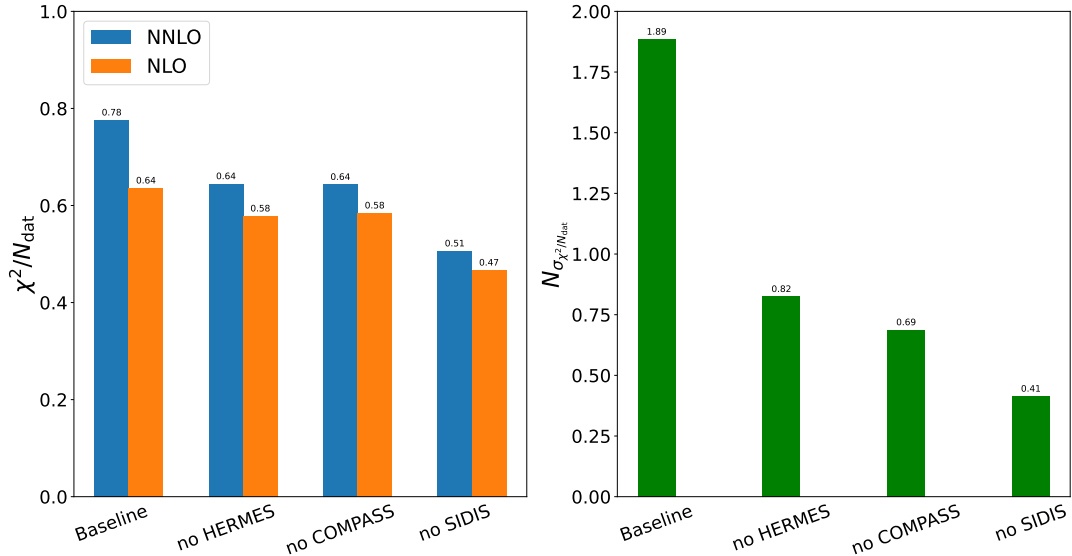


Figure 3. Left: The values of the global χ^2 per data point for the NLO and NNLO baseline fits compared to the corresponding values obtained excluding the HERMES SIDIS data, the COMPASS SIDIS data, and all SIDIS data. Right: The corresponding fraction of standard deviations in units of the χ^2 per data point of the difference between the NLO and NNLO χ^2 , $N_{\sigma_{\chi^2}}/N_{\text{dat}}$.

splitting in the perturbative evolution, almost unconstrained. Indeed, Δf_g only enters the DIS and SIDIS cross sections beyond leading order, therefore it is suppressed by a power of α_s with respect to the quark distributions. Moreover, scale violations due to PDF evolution, to which Δf_g is sensitive, are also small because of the limited coverage in Q^2 of the data.

5.2 Impact of data

In order to investigate the relationship between data sets and fit quality more closely, we assessed the relative impact of DIS and SIDIS data on PDFs by performing three pairs (NLO and NNLO) of variant fits to reduced data sets: a first pair from which we removed the COMPASS SIDIS data; a second pair from which we removed the HERMES SIDIS data; and a third pair from which we removed the SIDIS data altogether. In this last case, because inclusive DIS data alone is not sensitive to all of the PDF combinations in Eq. (9), we used the restricted parametrisation basis $\{\Delta f_u^+, \Delta f_d^+, \Delta f_s^+, \Delta f_g\}$, where $\Delta f_q^+ = \Delta f_q + \Delta f_{\bar{q}}$, with $q = u, d, s$.

In Fig. 3, we display, for all of these fits and for the baseline fits, the values of the global χ^2 per data point (left), and the fraction of standard deviations in units of χ^2 per data point corresponding to the difference between NLO and NNLO, defined as $N_{\sigma_{\chi^2}}/N_{\text{dat}} = (\chi_{\text{NNLO}}^2 - \chi_{\text{NLO}}^2)/\sqrt{2N_{\text{dat}}}$ (right). In all cases, the global χ^2 remains larger at NNLO than at NLO. However, $N_{\sigma_{\chi^2}}/N_{\text{dat}}$ reduces from about two to less than one when either the HERMES or the COMPASS SIDIS measurements are removed from the fit, and to one half when all SIDIS data is removed altogether from the fit. Therefore, in these three last cases the significance of the increase in χ^2 observed when including NNLO corrections is compatible with a one-sigma statistical fluctuation of the χ^2 . This analysis also suggests that there are two effects responsible for the deterioration of the fit quality upon inclusion of NNLO corrections: the fact that the SIDIS data sets are not described as well as the DIS ones; and the fact that HERMES and COMPASS SIDIS data sets, while being equally well described separately, are no longer so when included together in the fit. The latter fact, which may point towards an inconsistency between the two experiments, seems to lead to the largest deterioration of the fit quality.

In Fig. 4, we compare the Δf_u^+ , Δf_d^+ , Δf_s^+ , and Δf_g PDF combinations obtained in the baseline fits and in the fits with no SIDIS data included. The comparison is reported at $Q^2 = 10 \text{ GeV}^2$ for both NNLO and NLO. Error bands correspond to one-sigma uncertainties. We observe a non-trivial

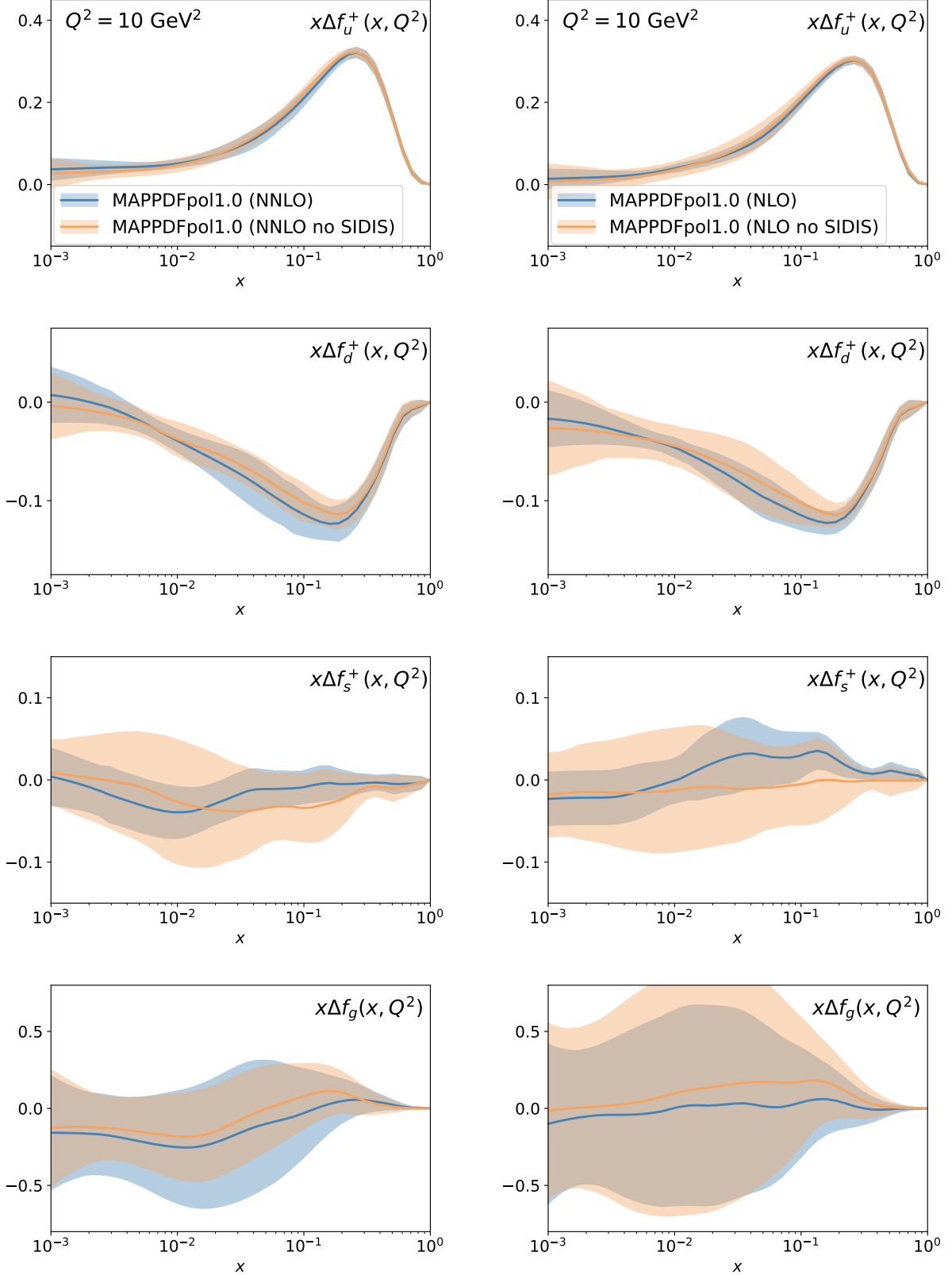


Figure 4. The Δf_u^+ , Δf_d^+ , Δf_s^+ , and Δf_g PDF combinations as functions of x at $Q^2 = 10 \text{ GeV}^2$ from the MAPPDFPOL1.0 NNLO (left) and NLO (right) PDF sets compared to the PDFs from the corresponding sets without SIDIS data. Error bands correspond to one-sigma uncertainties.

interplay between SIDIS data and NNLO corrections.

In the case of Δf_s^+ , SIDIS data has a consistent impact at NLO and NNLO, which results in a

reduction of PDF uncertainties by up to 50% for $0.01 \lesssim x \lesssim 0.1$. Interestingly, Δf_s^+ turns out to be compatible in the global determination and in the determination without SIDIS data. This is in contrast with previous analyses (see *e.g.* [65] and references therein) in which a tension between DIS and SIDIS data was claimed, with the former leading to a markedly negative Δf_s^+ and the latter to a sign-changing Δf_s^+ . We instead find results compatible with zero within large uncertainties in both cases, which are even more so upon inclusion of NNLO corrections. We believe that this is a consequence of the combination of our parametrisation, which is more flexible than that used in previous analyses, and of the usage of the MAPFF1.0 kaon FFs [24], which were determined with the same methodology used to determine the current PDFs.

In the case of Δf_u^+ and of Δf_d^+ , SIDIS data has a different impact at NLO and NNLO. At NLO, we observe a reduction of the uncertainties for all values of x ; at NNLO, instead, we observe an increase of the uncertainties for all values of x . We therefore conclude that the inclusion of NNLO corrections somewhat amplifies an underlying tension in the SIDIS data sets. Given that this behaviour is observed for Δf_u^+ and Δf_d^+ , but not for Δf_s^+ , we conclude that the pion data and FFs need further investigation, which we leave for a future study. Finally, as expected, Δf_g is left unaltered by SIDIS data at both NLO and NNLO.

5.3 Impact of theoretical constraints

We finally investigate the impact of including data for a_3 and a_8 and of imposing the positivity constraint. To this purpose, we performed three additional fits: two fits, one at NLO and one at NNLO, from which we removed the data points for a_3 and a_8 ; and one NNLO fit in which we set $K = 50$ in Eq. (14). This choice makes the positivity constraint so loose that it virtually corresponds to removing it altogether. The fit quality of each of these additional fits, as quantified by the χ^2 per data point, is reported in Table 1 for the individual and for the global data sets. The corresponding NNLO PDFs are displayed in Figs. 5 and 6: in Fig. 5, we compare the Δf_u , $\Delta f_{\bar{u}}$, Δf_d , $\Delta f_{\bar{d}}$, Δf_s , and $\Delta f_{\bar{s}}$ PDFs from the MAPPDFPOL1.0 NNLO PDF sets with and without a_3 and a_8 ; in Fig. 6, we compare the Δf_u , Δf_d , Δf_s , and Δf_g PDFs from the MAPPDFPOL1.0 NNLO PDF sets with and without the positivity constraint imposed. All comparisons are displayed as functions of x at $Q^2 = 10 \text{ GeV}^2$. Error bands correspond to one-sigma uncertainties.

Concerning the impact of the a_3 and a_8 data points, we see that it is negligible. The fit quality remains almost unaltered at both NLO and NNLO and so do PDF central values and uncertainties. We therefore conclude that the current DIS and SIDIS data does not point towards any significant violation of the SU(2) and SU(3) flavour symmetries. This finding is consistent with [64], where polarised PDFs and FFs were determined at NLO from a set of data very similar to ours.

Concerning the impact of the positivity constraint, we see that it is extremely relevant. Whereas the quality of the NNLO fit improves when removing it (incidentally, to a level close to that of the NLO fit with the positivity constraint), PDFs display peculiar shapes with large uncertainties in the large- x region. This is the region where the data is scarcer and where, therefore, the positivity constraint becomes dominant.

6 Summary and outlook

In this paper, we have presented MAPPDFPOL1.0, a new determination of the polarised PDFs of the proton from a global QCD analysis of the available DIS and SIDIS data. This determination includes, for the first time, NNLO QCD corrections to the DGLAP evolution equations and to the matrix elements of the two processes analysed. This determination has been carried out by extending the framework that we previously developed to determine the FFs of pions and kaons [23, 24]. It combines a neural-network parametrisation of PDFs with a Monte Carlo representation of their uncertainties, aiming at reducing parametrisation bias as much as possible and at obtaining statistically sound uncertainties.

Our main findings can be summarised as follows.

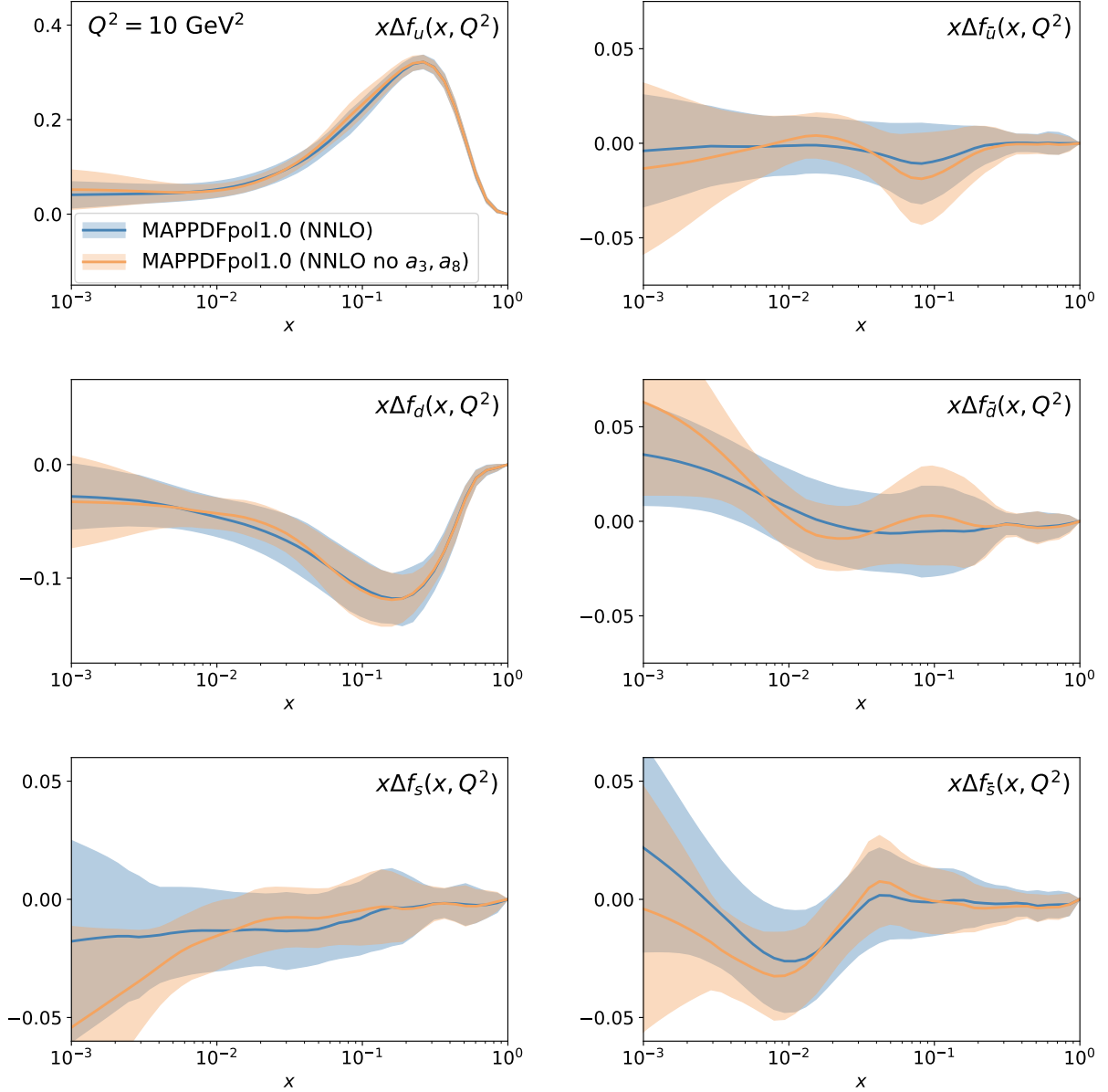


Figure 5. The Δf_u , $\Delta f_{\bar{u}}$, Δf_d , $\Delta f_{\bar{d}}$, Δf_s , and $\Delta f_{\bar{s}}$ PDFs as functions of x at $Q^2 = 10 \text{ GeV}^2$ from the MAPPDFPOL1.0 NNLO PDF sets with and without data for a_3 and a_8 included. Error bands correspond to one-sigma uncertainties.

- There is a subtle interplay between NNLO corrections and experimental data. Whereas all the data sets analysed are generally well described, the inclusion of NNLO corrections leads to a deterioration of the global fit quality up to two sigma in the χ^2 . This increase is observed also in fits without SIDIS data and in fits without either HERMES or COMPASS SIDIS data (at a level of about half a sigma), although the largest deterioration in the fit quality is seen when HERMES and COMPASS SIDIS measurements are simultaneously included in the fit. This behaviour, already observed when determining FFs from unpolarised SIDIS data [24], calls for further investigations both on the experimental side and on the accuracy of the approximate computation of NNLO corrections to the SIDIS cross sections. In this last respect, it was recently shown that the approximate computation of Ref. [18] is well reproduced by the exact computation [50] in the unpolarised case. A similar comparison in the polarised case will be beneficial when the exact computation will also be completed. The impact of NNLO corrections on PDFs is otherwise moderate, as they leave PDF central values almost unchanged, and lead

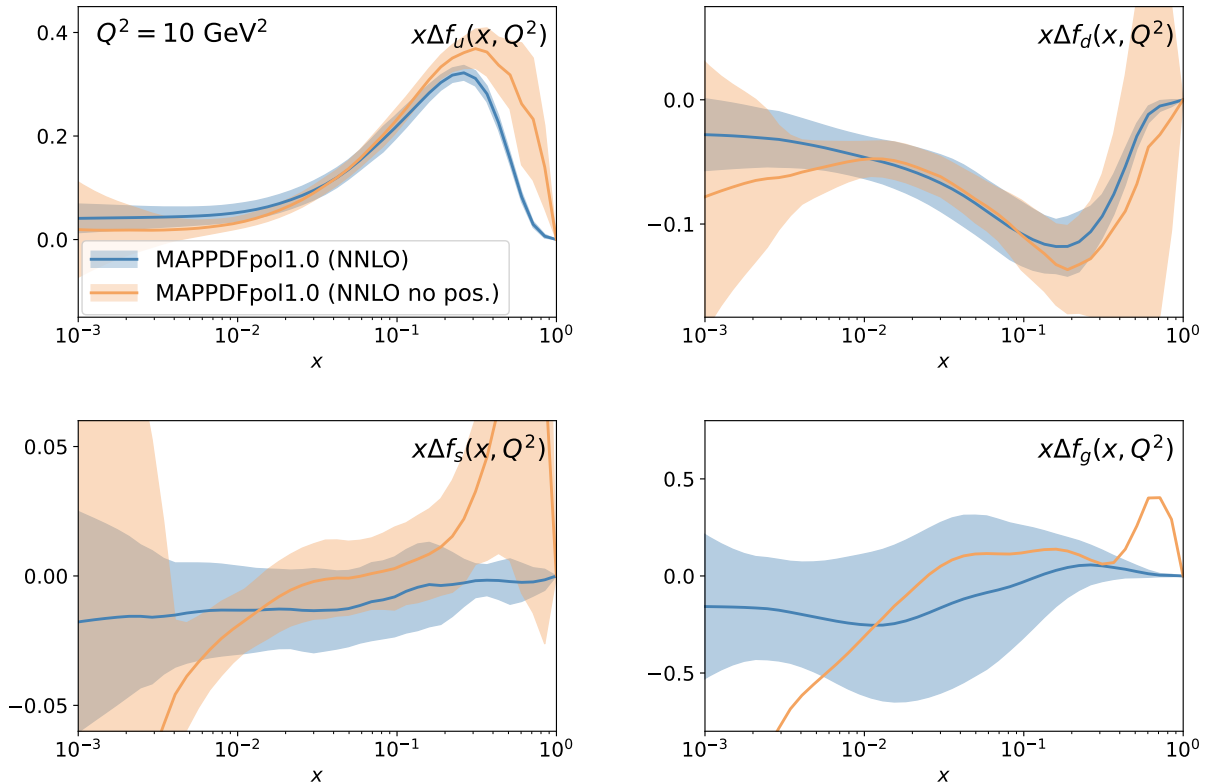


Figure 6. The Δf_u , Δf_d , Δf_s , and Δf_g , PDFs as functions of x at $Q^2 = 10 \text{ GeV}^2$ from the MAPPDFPOL1.0 NNLO PDF sets with and without the positivity constraint imposed. Error bands correspond to one-sigma uncertainties.

to a small reduction of uncertainties for the polarised strangeness and gluon PDFs.

- The analysed data is not able to constrain all parametrised PDFs to the same accuracy. Whereas the up- and down-quark polarised PDFs are generally well constrained and the SIDIS data moderately help pin down uncertainties, the sea-quark and gluon polarised PDFs remain largely unconstrained and essentially compatible with zero within their large uncertainties. The combination of SIDIS data for kaon production and NNLO corrections is not able to tell whether there is an asymmetry between strange quark and strange antiquark polarised PDFs, which in our analysis we parametrised independently for the first time. However, SIDIS data helps reduce uncertainties on these PDFs significantly. Noteworthy is the fact that the total polarised strange PDF turns out to be similar in the global determination and in the determination without SIDIS data, and in turn compatible with zero within uncertainties. This is in contrast with previous analyses (see *e.g.* Ref. [65]) in which a tension between DIS and SIDIS data was claimed, with the former leading to a markedly negative total polarised strange PDF and the latter to a sign-changing one. We ascribe this finding to the flexibility of our parametrisation in conjunction with the usage of the MAPFF1.0 kaon FF set [24] which was determined with the same methodology used to determine the current PDFs.
- The impact of theoretical constraints on the determination of polarised PDFs is variegated. On the one hand, the inclusion of data for a_3 and a_8 has negligible impact on both NLO and NNLO determinations: PDF central values and uncertainties remain almost unaffected. We therefore conclude that the current DIS and SIDIS data does not point towards any significant violation of the SU(2) and SU(3) flavour symmetries. The impact of the positivity constraint is instead very significant. While the quality of the NNLO fit improves when removing it, PDFs display peculiar shapes with large uncertainties in the large- x region.

Our analysis can be improved on two main fronts. First, by including hadronic data, specifically for gauge boson production, inclusive hadron production, and single-inclusive and double-inclusive jet production in polarised proton–proton collisions. The first process, for which NNLO corrections are known [19], can be used to validate polarised sea quark PDFs obtained from SIDIS. The other processes, being sensitive to the polarised gluon PDF starting from LO, are expected to be instrumental in determining the fraction of the proton spin carried by gluons. The second main front concerns an improvement of the theoretical treatment by means of the inclusion of theory uncertainties. In the spirit of recent analyses carried out for unpolarised PDFs [66–69], these are related to both missing higher-order corrections in the perturbative expansion and to nuclear corrections. The former may help assess the relevance of the NNLO corrections and to estimate the residual impact of contributions beyond NNLO. The latter may help understand how good the isospin approximation is when relating deuteron and proton structure functions.

In summary, our NNLO polarised PDF sets, being the only ones publicly available at this perturbative order to date, could be used in a number of applications that require a matching theoretical accuracy. For example, they can be employed to obtain accurate predictions for DIS and SIDIS cross sections to be measured at the future EIC, or they could serve as a baseline for the parametrisation and the determination of polarised transverse-momentum-dependent distributions at high accuracy.

The results presented in this paper have been obtained with the public code [29] available at

<https://github.com/MapCollaboration/Denali>,

with which we deliver our NLO and NNLO baseline polarised PDF sets in the LHAPDF format [28]. They are obtained from the a global data set that includes DIS and SIDIS measurements as well as the data for a_3 and a_8 , and they obey the positivity constraint in Eq. (10). The names of these PDF sets are:

- NLO: MAPPDFpo110NLO;
- NNLO: MAPPDFpo110NNLO.

They will also be released on the LHAPDF public repository. The variant PDF sets discussed in Sects. 5.2–5.3 are available from the authors upon request.

Acknowledgments

We thank Gunar Schnell for clarifications on the HERMES SIDIS data, Rabah Abdul Khalek for contributing to develop the numerical framework used in this analysis, and the members of the MAP Collaboration for comments on the draft. V. B. is supported by the European Union’s Horizon 2020 research and innovation programme under grant agreement STRONG 2020 - No 824093. E.R. N. is supported by the Italian Ministry of University and Research (MUR) through the “Rita Levi-Montalcini” Program.

References

- [1] J. J. Ethier and E. R. Nocera, *Parton Distributions in Nucleons and Nuclei*, *Ann. Rev. Nucl. Part. Sci.* **70** (2020) 43–76, [[arXiv:2001.07722](https://arxiv.org/abs/2001.07722)].
- [2] X. Ji, F. Yuan, and Y. Zhao, *What we know and what we don’t know about the proton spin after 30 years*, *Nature Rev. Phys.* **3** (2021), no. 1 27–38, [[arXiv:2009.01291](https://arxiv.org/abs/2009.01291)].
- [3] **European Muon** Collaboration, J. Ashman et al., *A Measurement of the Spin Asymmetry and Determination of the Structure Function $g(1)$ in Deep Inelastic Muon-Proton Scattering*, *Phys. Lett. B* **206** (1988) 364.

- [4] **European Muon** Collaboration, J. Ashman et al., *An Investigation of the Spin Structure of the Proton in Deep Inelastic Scattering of Polarized Muons on Polarized Protons*, *Nucl. Phys. B* **328** (1989) 1.
- [5] R. Abdul Khalek et al., *Science Requirements and Detector Concepts for the Electron-Ion Collider: EIC Yellow Report*, *Nucl. Phys. A* **1026** (2022) 122447, [[arXiv:2103.05419](#)].
- [6] R. Abdul Khalek et al., *Snowmass 2021 White Paper: Electron Ion Collider for High Energy Physics*, [arXiv:2203.13199](#).
- [7] I. Borsa, G. Lucero, R. Sassot, E. C. Aschenauer, and A. S. Nunes, *Revisiting helicity parton distributions at a future electron-ion collider*, *Phys. Rev. D* **102** (2020), no. 9 094018, [[arXiv:2007.08300](#)].
- [8] E. B. Zijlstra and W. L. van Neerven, *Order- α_s^2 corrections to the polarized structure function $g_1(x, Q^2)$* , *Nucl. Phys. B* **417** (1994) 61–100. [Erratum: *Nucl.Phys.B* 426, 245 (1994), Erratum: *Nucl.Phys.B* 773, 105–106 (2007), Erratum: *Nucl.Phys.B* 501, 599–599 (1997)].
- [9] I. Borsa, D. de Florian, and I. Pedron, *The full set of polarized deep inelastic scattering structure functions at NNLO accuracy*, *Eur. Phys. J. C* **82** (2022), no. 12 1167, [[arXiv:2210.12014](#)].
- [10] J. Blümlein, P. Marquard, C. Schneider, and K. Schönwald, *The massless three-loop Wilson coefficients for the deep-inelastic structure functions F_2 , F_L , xF_3 and g_1* , *JHEP* **11** (2022) 156, [[arXiv:2208.14325](#)].
- [11] F. Hekhorn and M. Stratmann, *Next-to-Leading Order QCD Corrections to Inclusive Heavy-Flavor Production in Polarized Deep-Inelastic Scattering*, *Phys. Rev. D* **98** (2018), no. 1 014018, [[arXiv:1805.09026](#)].
- [12] A. Behring, J. Blümlein, A. De Freitas, A. von Manteuffel, and C. Schneider, *The 3-Loop Non-Singlet Heavy Flavor Contributions to the Structure Function $g_1(x, Q^2)$ at Large Momentum Transfer*, *Nucl. Phys. B* **897** (2015) 612–644, [[arXiv:1504.08217](#)].
- [13] J. Ablinger, A. Behring, J. Blümlein, A. De Freitas, A. von Manteuffel, C. Schneider, and K. Schönwald, *The three-loop single mass polarized pure singlet operator matrix element*, *Nucl. Phys. B* **953** (2020) 114945, [[arXiv:1912.02536](#)].
- [14] A. Behring, J. Blümlein, A. De Freitas, A. von Manteuffel, K. Schönwald, and C. Schneider, *The polarized transition matrix element $A_{gq}(N)$ of the variable flavor number scheme at $O(\alpha_s^3)$* , *Nucl. Phys. B* **964** (2021) 115331, [[arXiv:2101.05733](#)].
- [15] J. Blümlein, A. De Freitas, M. Saragnese, C. Schneider, and K. Schönwald, *Logarithmic contributions to the polarized $O(\alpha_s^3)$ asymptotic massive Wilson coefficients and operator matrix elements in deeply inelastic scattering*, *Phys. Rev. D* **104** (2021), no. 3 034030, [[arXiv:2105.09572](#)].
- [16] I. Bierenbaum, J. Blümlein, A. De Freitas, A. Goedicke, S. Klein, and K. Schönwald, *$O(\alpha_s^2)$ polarized heavy flavor corrections to deep-inelastic scattering at $Q^2 \gg m^2$* , *Nucl. Phys. B* **988** (2023) 116114, [[arXiv:2211.15337](#)].
- [17] J. Ablinger, A. Behring, J. Blümlein, A. De Freitas, A. von Manteuffel, C. Schneider, and K. Schönwald, *The first-order factorizable contributions to the three-loop massive operator matrix elements $A_{Qg}^{(3)}$ and $\Delta A_{Qg}^{(3)}$* , [arXiv:2311.00644](#).
- [18] M. Abele, D. de Florian, and W. Vogelsang, *Approximate NNLO QCD corrections to semi-inclusive DIS*, *Phys. Rev. D* **104** (2021), no. 9 094046, [[arXiv:2109.00847](#)].

- [19] R. Boughezal, H. T. Li, and F. Petriello, *W-boson production in polarized proton-proton collisions at RHIC through next-to-next-to-leading order in perturbative QCD*, *Phys. Lett. B* **817** (2021) 136333, [[arXiv:2101.02214](#)].
- [20] F. Taghavi-Shahri, H. Khanpour, S. Atashbar Tehrani, and Z. Alizadeh Yazdi, *Next-to-next-to-leading order QCD analysis of spin-dependent parton distribution functions and their uncertainties: Jacobi polynomials approach*, *Phys. Rev. D* **93** (2016), no. 11 114024, [[arXiv:1603.03157](#)].
- [21] D. de Florian, R. Sassot, M. Stratmann, and W. Vogelsang, *Evidence for polarization of gluons in the proton*, *Phys. Rev. Lett.* **113** (2014), no. 1 012001, [[arXiv:1404.4293](#)].
- [22] **NNPDF** Collaboration, E. R. Nocera, R. D. Ball, S. Forte, G. Ridolfi, and J. Rojo, *A first unbiased global determination of polarized PDFs and their uncertainties*, *Nucl. Phys. B* **887** (2014) 276–308, [[arXiv:1406.5539](#)].
- [23] **MAP (Multi-dimensional Analyses of Partonic distributions)** Collaboration, R. A. Khalek, V. Bertone, and E. R. Nocera, *Determination of unpolarized pion fragmentation functions using semi-inclusive deep-inelastic-scattering data*, *Phys. Rev. D* **104** (2021), no. 3 034007, [[arXiv:2105.08725](#)].
- [24] **MAP (Multi-dimensional Analyses of Partonic distributions)** Collaboration, R. Abdul Khalek, V. Bertone, A. Khoudli, and E. R. Nocera, *Pion and kaon fragmentation functions at next-to-next-to-leading order*, *Phys. Lett. B* **834** (2022) 137456, [[arXiv:2204.10331](#)].
- [25] **NNPDF** Collaboration, R. D. Ball et al., *The path to proton structure at 1% accuracy*, *Eur. Phys. J. C* **82** (2022), no. 5 428, [[arXiv:2109.02653](#)].
- [26] R. Abdul Khalek, R. Gauld, T. Giani, E. R. Nocera, T. R. Rabemananjara, and J. Rojo, *nNNPDF3.0: evidence for a modified partonic structure in heavy nuclei*, *Eur. Phys. J. C* **82** (2022), no. 6 507, [[arXiv:2201.12363](#)].
- [27] **NNPDF** Collaboration, V. Bertone, S. Carrazza, N. P. Hartland, E. R. Nocera, and J. Rojo, *A determination of the fragmentation functions of pions, kaons, and protons with faithful uncertainties*, *Eur. Phys. J. C* **77** (2017), no. 8 516, [[arXiv:1706.07049](#)].
- [28] A. Buckley, J. Ferrando, S. Lloyd, K. Nordström, B. Page, M. Rufenacht, M. Schönherr, and G. Watt, *LHAPDF6: parton density access in the LHC precision era*, *Eur. Phys. J. C* **75** (2015) 132, [[arXiv:1412.7420](#)].
- [29] V. Bertone, A. Chiefa, and E. R. Nocera, *Mapcollaboration/denali: Sheldon chalet*, Apr., 2024.
- [30] **Spin Muon** Collaboration, B. Adeva et al., *Spin asymmetries $A(1)$ and structure functions g_1 of the proton and the deuteron from polarized high-energy muon scattering*, *Phys. Rev. D* **58** (1998) 112001.
- [31] **COMPASS** Collaboration, C. Adolph et al., *The spin structure function g_1^p of the proton and a test of the Bjorken sum rule*, *Phys. Lett. B* **753** (2016) 18–28, [[arXiv:1503.08935](#)].
- [32] **COMPASS** Collaboration, C. Adolph et al., *Final COMPASS results on the deuteron spin-dependent structure function g_1^d and the Bjorken sum rule*, *Phys. Lett. B* **769** (2017) 34–41, [[arXiv:1612.00620](#)].
- [33] **E142** Collaboration, P. L. Anthony et al., *Deep inelastic scattering of polarized electrons by polarized He-3 and the study of the neutron spin structure*, *Phys. Rev. D* **54** (1996) 6620–6650, [[hep-ex/9610007](#)].

- [34] **E143** Collaboration, K. Abe et al., *Measurements of the proton and deuteron spin structure functions $g(1)$ and $g(2)$* , *Phys. Rev. D* **58** (1998) 112003, [[hep-ph/9802357](#)].
- [35] **E154** Collaboration, K. Abe et al., *Precision determination of the neutron spin structure function $g_1(n)$* , *Phys. Rev. Lett.* **79** (1997) 26–30, [[hep-ex/9705012](#)].
- [36] **E155** Collaboration, P. L. Anthony et al., *Measurements of the Q^{*2} dependence of the proton and neutron spin structure functions $g(1)^{*p}$ and $g(1)^{*n}$* , *Phys. Lett. B* **493** (2000) 19–28, [[hep-ph/0007248](#)].
- [37] **HERMES** Collaboration, K. Ackerstaff et al., *Measurement of the neutron spin structure function $g_1(n)$ with a polarized He-3 internal target*, *Phys. Lett. B* **404** (1997) 383–389, [[hep-ex/9703005](#)].
- [38] **HERMES** Collaboration, A. Airapetian et al., *Precise determination of the spin structure function $g(1)$ of the proton, deuteron and neutron*, *Phys. Rev. D* **75** (2007) 012007, [[hep-ex/0609039](#)].
- [39] **Jefferson Lab Hall A** Collaboration, D. Flay et al., *Measurements of d_2^n and A_1^n : Probing the neutron spin structure*, *Phys. Rev. D* **94** (2016), no. 5 052003, [[arXiv:1603.03612](#)].
- [40] **CLAS** Collaboration, Y. Prok et al., *Precision measurements of g_1 of the proton and the deuteron with 6 GeV electrons*, *Phys. Rev. C* **90** (2014), no. 2 025212, [[arXiv:1404.6231](#)].
- [41] **NNPDF** Collaboration, R. D. Ball, S. Forte, A. Guffanti, E. R. Nocera, G. Ridolfi, and J. Rojo, *Unbiased determination of polarized parton distributions and their uncertainties*, *Nucl. Phys. B* **874** (2013) 36–84, [[arXiv:1303.7236](#)].
- [42] **COMPASS** Collaboration, M. G. Alekseev et al., *Quark helicity distributions from longitudinal spin asymmetries in muon-proton and muon-deuteron scattering*, *Phys. Lett. B* **693** (2010) 227–235, [[arXiv:1007.4061](#)].
- [43] **HERMES** Collaboration, A. Airapetian et al., *Longitudinal double-spin asymmetries in semi-inclusive deep-inelastic scattering of electrons and positrons by protons and deuterons*, *Phys. Rev. D* **99** (2019), no. 11 112001, [[arXiv:1810.07054](#)].
- [44] **Jefferson Lab Hall A** Collaboration, X. Zheng et al., *Precision measurement of the neutron spin asymmetries and spin-dependent structure functions in the valence quark region*, *Phys. Rev. C* **70** (2004) 065207, [[nucl-ex/0405006](#)].
- [45] **CLAS** Collaboration, N. Guler et al., *Precise determination of the deuteron spin structure at low to moderate Q^2 with CLAS and extraction of the neutron contribution*, *Phys. Rev. C* **92** (2015), no. 5 055201, [[arXiv:1505.07877](#)].
- [46] P. G. Ratcliffe, *Hyperon beta decay and the CKM matrix*, *Czech. J. Phys.* **54** (2004) B11–B20, [[hep-ph/0402063](#)].
- [47] **Particle Data Group** Collaboration, R. L. Workman et al., *Review of Particle Physics*, *PTEP* **2022** (2022) 083C01.
- [48] W. Furmanski and R. Petronzio, *Lepton - Hadron Processes Beyond Leading Order in Quantum Chromodynamics*, *Z. Phys. C* **11** (1982) 293.
- [49] D. de Florian, M. Stratmann, and W. Vogelsang, *QCD analysis of unpolarized and polarized Lambda baryon production in leading and next-to-leading order*, *Phys. Rev. D* **57** (1998) 5811–5824, [[hep-ph/9711387](#)].
- [50] L. Bonino, T. Gehrmann, and G. Stagnitto, *Semi-inclusive deep-inelastic scattering at NNLO in QCD*, [[arXiv:2401.16281](#)].

- [51] F. Hekhorn, G. Magni, E. R. Nocera, T. R. Rabemananjara, J. Rojo, A. Schaus, and R. Stegeman, *Heavy quarks in polarised deep-inelastic scattering at the electron-ion collider*, *Eur. Phys. J. C* **84** (2024), no. 2 189, [[arXiv:2401.10127](#)].
- [52] S. Moch, J. A. M. Vermaseren, and A. Vogt, *The Three-Loop Splitting Functions in QCD: The Helicity-Dependent Case*, *Nucl. Phys. B* **889** (2014) 351–400, [[arXiv:1409.5131](#)].
- [53] S. Moch, J. A. M. Vermaseren, and A. Vogt, *On γ_5 in higher-order QCD calculations and the NNLO evolution of the polarized valence distribution*, *Phys. Lett. B* **748** (2015) 432–438, [[arXiv:1506.04517](#)].
- [54] J. Blümlein, P. Marquard, C. Schneider, and K. Schönwald, *The three-loop polarized singlet anomalous dimensions from off-shell operator matrix elements*, *JHEP* **01** (2022) 193, [[arXiv:2111.12401](#)].
- [55] **APFEL** Collaboration, V. Bertone, S. Carrazza, and J. Rojo, *APFEL: A PDF Evolution Library with QED corrections*, *Comput. Phys. Commun.* **185** (2014) 1647–1668, [[arXiv:1310.1394](#)].
- [56] V. Bertone, *APFEL++: A new PDF evolution library in C++*, *PoS DIS2017* (2018) 201, [[arXiv:1708.00911](#)].
- [57] G. Altarelli, S. Forte, and G. Ridolfi, *On positivity of parton distributions*, *Nucl. Phys. B* **534** (1998) 277–296, [[hep-ph/9806345](#)].
- [58] D. de Florian, S. Forte, and W. Vogelsang, *Higgs production at RHIC and the positivity of the gluon helicity distribution*, [[arXiv:2401.10814](#)].
- [59] **NNPDF** Collaboration, R. D. Ball et al., *Parton distributions from high-precision collider data*, *Eur. Phys. J. C* **77** (2017), no. 10 663, [[arXiv:1706.00428](#)].
- [60] S. Agarwal, K. Mierle, and T. C. S. Team, *Ceres Solver*, 10, 2023.
- [61] R. Abdul Khalek and V. Bertone, *On the derivatives of feed-forward neural networks*, [[arXiv:2005.07039](#)].
- [62] I. Borsa, R. Sassot, D. de Florian, M. Stratmann, and W. Vogelsang, *Towards a Global QCD Analysis of Fragmentation Functions at Next-to-Next-to-Leading Order Accuracy*, *Phys. Rev. Lett.* **129** (2022), no. 1 012002, [[arXiv:2202.05060](#)].
- [63] D. De Florian, G. A. Lucero, R. Sassot, M. Stratmann, and W. Vogelsang, *Monte Carlo sampling variant of the DSSV14 set of helicity parton densities*, *Phys. Rev. D* **100** (2019), no. 11 114027, [[arXiv:1902.10548](#)].
- [64] J. J. Ethier, N. Sato, and W. Melnitchouk, *First simultaneous extraction of spin-dependent parton distributions and fragmentation functions from a global QCD analysis*, *Phys. Rev. Lett.* **119** (2017), no. 13 132001, [[arXiv:1705.05889](#)].
- [65] E. Leader, A. V. Sidorov, and D. B. Stamenov, *New analysis concerning the strange quark polarization puzzle*, *Phys. Rev. D* **91** (2015), no. 5 054017, [[arXiv:1410.1657](#)].
- [66] **NNPDF** Collaboration, R. Abdul Khalek et al., *A first determination of parton distributions with theoretical uncertainties*, *Eur. Phys. J. C* (2019) 79:838, [[arXiv:1905.04311](#)].
- [67] **NNPDF** Collaboration, R. Abdul Khalek et al., *Parton Distributions with Theory Uncertainties: General Formalism and First Phenomenological Studies*, *Eur. Phys. J. C* **79** (2019), no. 11 931, [[arXiv:1906.10698](#)].

- [68] **NNPDF** Collaboration, R. D. Ball et al., *Determination of the theory uncertainties from missing higher orders on NNLO parton distributions with percent accuracy*, [arXiv:2401.10319](#).
- [69] R. D. Ball, E. R. Nocera, and R. L. Pearson, *Deuteron Uncertainties in the Determination of Proton PDFs*, *Eur. Phys. J. C* **81** (2021), no. 1 37, [[arXiv:2011.00009](#)].